Biophysical Chemistry 18 (1983) 211–223
Elsevier

BPC 00800

EXPERIMENTAL STUDY OF SYNCHRONIZATION PHENOMENA UNDER PERIODIC LIGHT IRRADIATION OF A NONLINEAR CHEMICAL SYSTEM

Etiennette DULOS and Patrick DE KEPPER

Centre de Recherche Paul Pascal, CNRS, University of Bordeaux I, Domaine Universitaire, 33405 Talence Cedex, France

Received 28th December 1982
Revised manuscript received 30th May 1983
Accepted 31st May 1983

Key words: Nonlinear dynamical system; Oscillation; Excitability; Multistability; Phase locking; Synchronization; Phase resetting curve

A photosensitive chemical oscillating reaction, i.e., the Briggs-Rauscher (B.R.) reaction, exhibiting a wealth of nonlinear behavior, when performed in a continuous-flow stirred-tank reactor, and subjected to periodic light irradiation, is studied as an experimental example of entrainment phenomena observable in biological systems. The adaptation patterns under periodic light irradiation are elucidated by means of the response of the system to continuous and single-pulse light irradiation. It is shown that self-oscillating states, excitable steady states and bistable systems can exhibit the same types of synchronization patterns when submitted to periodic external forces with appropriate amplitude and time scale conditions.

1. Introduction

Synchronization of oscillators, a thoroughly studied phenomenon in physics, has also been holding biologists' attention for several decades. It is often referred to as 'entrainment of biological rhythms' by periodic stimuli. These stimuli can be seasonal, circadian or may originate from endogenous metabolic and electrical oscillations, thus screening a very broad spectrum of frequencies. Synchronization can play a prominent part in regulation processes. For example, a wide variety of unicellular systems with autonomous circadian clocks exhibit light entrainment phenomena in the onset and modulation of their cell division and other physiological activities [1]. Another interesting example is the perception of seasons by many plants [2]: adaptation of Crassulacean to extreme climatic conditions [3] has been shown to be governed by seasonal changes in the time interval between day and night stimuli, each controling a specific enzymatic rhythm. Unfortunately, owing to the existence of very complex interaction networks in biological systems, it is very hard to analyze the interaction between biological oscillators.

The situation is much easier in purely chemical systems where self-oscillatory systems can currently be performed in very well defined environments, free of large uncontrolled fluctuations.

In the following, we describe the results obtained with such a chemical system, namely, the Briggs-Rauscher oscillating reaction [4], when submitted to periodic light pulses. No reference shall be made here to any underlying kinetic mechanism elucidated elsewhere [5a,5b]. This study can be thought of as an attempt to provide a chemical experimental model for less tractable biological systems submitted to external stimuli. Though the chemical species involved in chemistry and in biochemistry are quite different, the nonlinearities implicated in both systems are of the same type, as they derive from mass-action kinetics.

The Briggs-Rauscher reaction has been chosen

because of its high photosensitivity but also for its rich and well established phenomenology [6–8] when performed in a continuous-flow stirred-tank reactor. Indeed, depending on the constraint values, this reaction exhibits different stationary and oscillating states, hysteresis and excitability phenomena. This allows us to study various modes of entrainment in nonlinear chemical systems. The different constraints in this system are the input flow concentrations of the reagents (malonic acid, potassium iodate, hydrogen peroxide, manganese sulfate, perchloric acid), temperature (T), residence time (θ_r) of the chemical species in the reactor and, more specific to the present work, a light flux. The effects of light pulses were investigated on several different oscillating states, stationary excitable states and on a bistable situation.

The experimental setup (fig. 1) designed for this purpose includes the conventional continuous-flow stirred-tank reactor and a light source with its optical devices for irradiation of the reactor at 460 nm, a wavelength corresponding to the maximum absorption of iodine, an important chemical species produced by the reaction. The light flux is adjusted by means of a diaphragm. A shutter located at a focus point of the beam is driven by an electronic clock. Opening and closing times (i.e., illumination and extinction times) range from 1/10 to 1000 s. Two values were simultaneously recorded: the chemical potential (E) of a platinum electrode immersed in the reaction mixture and

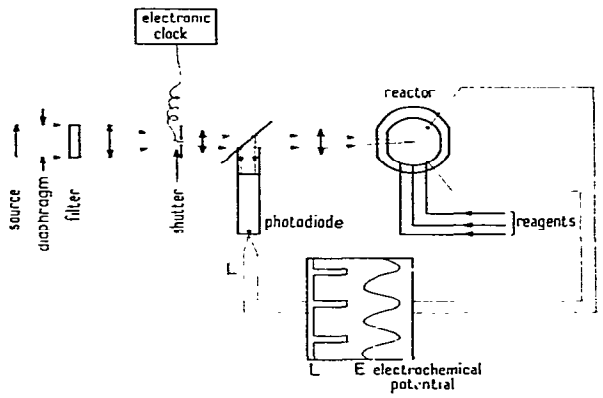

Fig. 1. The experimental setup.

light flux (L) of a tenuous beam derived from the main incident beam. Note that the potential cannot be related to any particular chemical species but it is a reliable measurement of the chemical state of the system. Note also that the proportionality of L to the flux that effectively irradiates the reactor has been checked by actinometry measurements. In the following, the L values are expressed in arbitrary units ($L = 1$ corresponds to 1.5×10^{16} photons/s entering the reactor). The light pulses obtained with the shutter are square pulses. They can be applied either isolated or periodically. The periodic light pulses are conveniently described by four independent parameters: P_L, the photoperiod; ΔL, the amplitude of the light flux jumps, i.e., the difference between the two extreme values (L_{max} and L_{min}) of the light flux during one photoperiod; ρ, the ratio of the maximum irradiation time to the photoperiod; and $\bar{L}$, the mean light flux during the whole photoperiod.

2. Effect of periodic light irradition on oscillating states

Several different oscillating chemical compositions were examined during this work [9] but only two quite different types of adaptation to a periodically changing environment were observed. We thus present here the effects of periodic illumination on only two typically different compositions. The first composition, referred to as β, ($[KIO_3]_0 = 0.048$ mole/l, $[H_2O_2]_0 = 0.33$ mol/l, $[CH_2(COOH)_2]_0 = 0.003$ mol/l, $[MnSO_4]_0 = 0.004$ mol/l, $[HClO_4]_0 = 0.056$ mol/l; $T = 20°C$, $\theta_r = 2.5$ min), corresponds to a typical relaxation oscillator. The second composition, referred to as α, ($[KIO_3]_0 = 0.048$ mol/l, $[H_2O_2]_0 = 0.33$ mol/l, $[CH_2(COOH)_2]_0 = 0.50$ mol/l, $[MnSO_4]_0 = 0.004$ mol/l, $[HClO_4]_0 = 0.056$ mol/l; $T = 40°C$, $\theta_r = 2.5$ min), corresponds to quasi-harmonic oscillations found imediately beyond a supercritical Hopf bifurcation [10]. In all cases, the concentrations are given for the reactor mixture prior to any reaction.

In order to understand clearly the different aspects of the light sensitivity of the reaction, we first examine briefly the effects of continuous light irradiation, before analyzing in a second set of

experiments the response to an isolated light pulse and finally investigate the consequence of periodic light pulses.

2.1. Effect of continuous light irradiation

Continuous light irradiation has two major effects on the oscillations of composition β (fig. 2). It reduces their amplitude and period. The measured chemical period (P_{ch}) of oscillations at increasing light flux L values is: $P_{ch}^{L=0} = 141$ s, $P_{ch}^{L=3} = 72$ s and $P_{ch}^{L=6} = 54$ s. Eventually, oscillations are completely abolished beyond a given L value, and the previously oscillating state gives way to a stationary state. This transition from the oscillatory state to a steady state is found to be reversible as a function of the light flux.

Composition α is much less sensitive to light irradiation: the period of oscillations remains unchanged ($P_{ch}^{L=0} = P_{ch}^{L=10} = 5.84$ s) and the amplitude of the potential oscillations is slightly reduced when L is changed from 0 to 20.

Thus, the influence of constant light irradiation clearly shows that changes in the light flux perturb more or less radically the chemical oscillator. After irradation is stopped, the oscillator returns to its original amplitude and period, thus manifesting its asymptotic stability. However, a permanent phase shift will generally result between the actual phase and the virtual phase this oscillator would have if it had remained unperturbed.

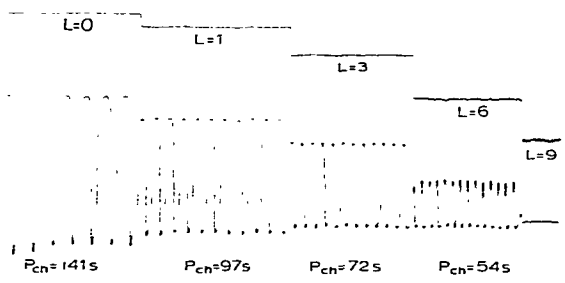

Fig. 2. Effects of continuous irradiation on the relaxation oscillations of composition β. Amplitude and period decrease as L is increased. At $L = 9$, the system no longer oscillates.

2.2. Effect of an isolated light pulse

For the analysis of our perturbation experiments, i.e., when one temporary perturbation is applied to the oscillator, we use terms and definitions usually adopted for perturbation experiments of biological oscillators [11,12]: Let ϕ, the phase of an event, be defined by $\Delta t/P_{ch}^{*}$, i.e., the ratio of the time Δt elapsed between this event and an arbitrary reference event – e.g., an extremum of the potential E – to the autonomous chemical period P_{ch}^{*}. The phase of the reference event is then $\phi = 0$. The next reference event is at $\phi = 1$ or $\phi = 0$ (modulo 1). $\Delta\phi$ is the normalized phase shift resulting from one temporary perturbation. It can be measured as shown in fig. 3. The $\Delta\phi$ value depends on two factors, the 'size' of the perturbation and the phase ϕ at which it is delivered.

In our perturbation experiments, the autonomous period was measured in continuous darkness. During each set of experiments, the amplitude ΔL of the light pulse was kept constant but the pulse duration S was changed. For a given pulse duration, the perturbation was applied at different ϕ values ($0 \leqslant \phi \leqslant 1$). The residual phase shift corresponding to every phase was measured after recovery of the autonomous period. As a practical matter, the oscillator had fully recovered after only four or five oscillations following the light pulse delivery.

For each S value, the $\Delta\phi$vs. ϕ phase-response

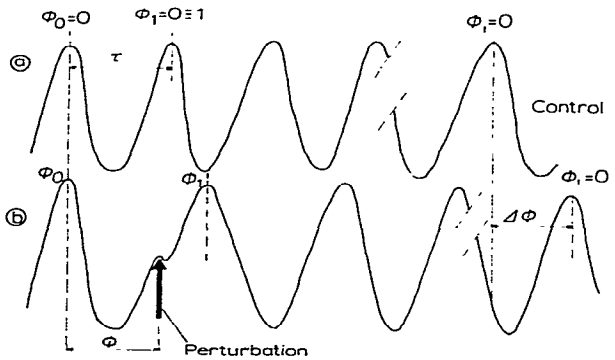

Fig. 3. Measuring method for the phase shift. (a) Virtual unperturbed oscillator, (b) perturbed oscillator.

curve was plotted. Fig. 4 exhibits a series of phase-response curves obtained on composition β for different durations S of the perturbation, with $\Delta L = 1$. In our convention, $\Delta\phi$ is positive when the new reference event is retarded and negative when advanced. At short values of S (fig. 4a and b), there is a significant zone where $\Delta\phi$ values are virtually zero irrespective of the phase, this is the so-called 'refractory zone'. The shorter S is, the longer is this refractory zone. Beyond the latter, the curve shows a discontinuity. $\Delta\phi$ becomes negative and rises again smoothly as ϕ is increased to unity. This is the 'sensitive zone' of the oscillation. The discontinuity of $\Delta\phi$ at the borderline between the refractory and sensitive zones reveals the excitable character of this oscillator. As seen in fig. 4a, the most sensitive zone of the oscillation immediately precedes the chosen reference event (minimum of potential). At long perturbations (fig. 4d), the refractory zone completely disappears and the response curve is composed of two segments of a straight line with a slope of unity, separated by exactly one period. The first part corresponds to a delay-inducing zone and the second to an advance-inducing zone. The intermediate duration, $S = 8$ s (fig. 4c), gives rise to a more complex situation where a small refractory zone is immediately followed by a delay-inducing zone which becomes suddenly interrupted. Beyond the discontinuity extends the advance-inducing zone.

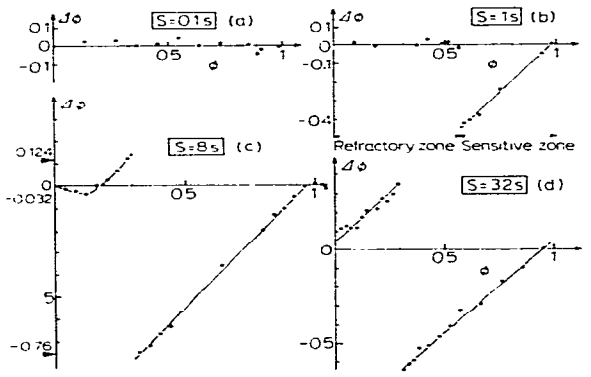

Fig. 4. Phase response curves ($\Delta\phi$ vs. ϕ), obtained on oscillations of composition β with $\Delta L = 1$, for four different perturbation durations S: (a) $S = 0.1$ s, (b) $S = 1$ s, (c) $S = 8$ s, (d) $S = 32$ s.

One of the major interests in phase-response curves is that they can be used to predict the synchronization capability of the oscillator when the same perturbation is periodically applied. These prediction properties have been mainly used for biological oscillators such as neuronal [13] and cardiac [12] pacemakers. Indeed, it can be shown [13] that, provided the oscillator recovers over a single ocsillation, the stable fundamental synchronization domains correspond to $\Delta\phi$ values for which the phase-response curve has a slope between 0 and 2. This has been checked for several S values on chemical composition β. For example, it can be seen in fig. 4c that the phase-response curve obtained at $S = 8$ s has a slope of 1 for $-0.76 \pm 0.02 \leqslant \Delta\phi \leqslant 0 \pm 0.008$, and a slope of 1.38 for $-0.032 \pm 0.008 \leqslant \Delta\phi \leqslant 0.124 \pm 0.02$. Knowing that the domains of direct synchronization are given by the following relationship:

$$P_L = P_{ch}^{*}(\Delta\phi + 1)$$

the resulting domain of P_L values providing direct synchronization of the chemical oscillator is 27 ± 2.5 s $\leqslant P_L \leqslant 142 \pm 3$ s. Note that to positive $\Delta\phi$ values correspond fundamental forced oscillations with periods greater than P_{ch}^{*}, the autonomous period, while to negative $\Delta\phi$ values correspond fundamental forced oscillations with periods shorter than P_{ch}^{*}. Outside the above-mentioned $\Delta\phi$ regions, no entrainment at $P_{ch} = P_L$ is possible. These values are in very good agreement with the actual experimentally observed limits of direct synchronization (from 26 ± 1 s to 135 ± 5 s). Outside this region, more complex entrainment patterns take place as shall be seen later. Further relationships between synchronization phenomena and information from phase-response curves are given in section 2.3.2.

2.3. Effect of periodic light pulses

2.3.1. On quasi-harmonic oscillations of composition α

Continuous light irradiation barely affects the potential oscillations of composition α, but periodic light pulses can produce dramatic changes in the oscillation pattern as illustrated in fig. 5. Remember that the quasi-harmonic oscillations have

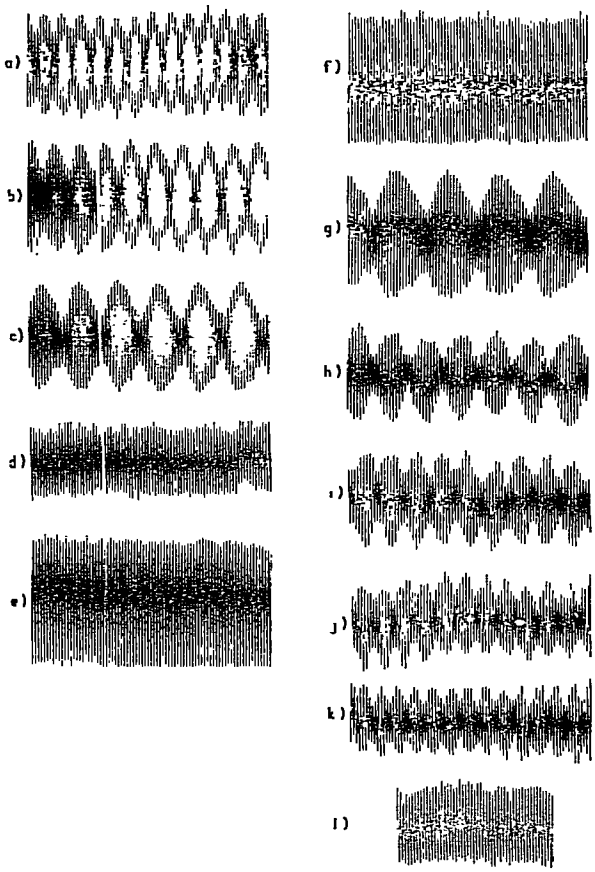

Fig. 5. Effects of periodic light pulses (period P_L) on the quasi-harmonic oscillations of composition α (autonomous period $P^*_{ch} = 5.84$ s): (a) $P_L = 5.0$ s, (b) $P_L = 5.2$ s, (c) $P_L = 5.4$ s, (d) $P_L = 5.6$ s, (e) $P_L = 5.8$ s, (f) $P_L = 6$ s, (g) $P_L = 6.2$ s, (h) $P_L = 6.4$ s, (i) $P_L = 6.6$ s, (j) $P_L = 6.8$ s, (k) $P_L = 7$ s, (l) $P_L = 7.4$ s. Direct synchronization is only observed under conditions d–f.

an autonomous period $P^*_{ch} = 5.84$ s in continuous darkness. The light parameters values chosen for periodic light irradiation were: $\rho = 1/2$, $L_{max} = 20$ and $L_{min} = 0$.

At P_L close to the autonomous period, chemical oscillations and periodic light pulses exactly synchronize ($P_{ch} = P_L$). However, this synchronization domain only extends to the immediate vicinity of the autonomous period value, for $5.6 \text{ s} \leqslant P_L \leqslant 6$ s (see fig. 5d–f).

Outside this narrow domain, a phenomenon analogous to 'beating' appears. The photoperiod is no longer able to synchronize the chemical period. The observed packs of oscillations result from a regular modulation of the amplitude and slight variations of the period. The mean chemical period $\bar{P}_{ch}$ measured inside any pack stays very close to the autonomous period. The maximum variation never exceeds 1%. Moreover, to some extent, the observed phenomenon obeys the 'law of the beating' concerning harmonic oscillators. The closer P_L is to P^*_{ch}, the larger are the packs of oscillations. Far enough from the synchronization domain, packs are no longer experimentally observed (see fig. 5l). The domain of observable oscillation packs extends between $P_L = 4.6$ and 7 s. Beyond these limits, no amplitude modulation can be seen and the measured P_{ch} never departs from the autonomous period.

2.3.2. On relaxation oscillations of composition β

Continuous light irradiation and isolated light pulses have already shown the high light sensitivity and the excitability property of these oscillations. They are also very sensitive to periodic perturbations. Because of this light sensitivity, the study was done at constant mean light irradiation $\bar{L}$ and, in the following, we shall term 'free-running period' $P^{\bar{L}}_{ch}$ the period of the oscillation under constant light irradiation at $L = \bar{L}$. The chemical period measured under periodic irradiation at the same mean flux $\bar{L}$ will be compared to this free-running period. The parameter ρ was held at a constant value of 1/4. Experiments were performed at constant ΔL and $\bar{L}$. P_L was incresaed from a few tenths of second to about 200 s.

In composition β, the periodic light pulses are able to induce a great variety of synchronization patterns. Within our experimental accuracy, all these synchronization patterns consisted of 'm' chemical oscillations during 'n' photoperiods, where m and n are any two integers. For convenience, we may distinguish two different types of synchronization, those for which $m = 1$ and those more complex where $m > 1$, i.e., repetitive patterns involving, respectively, one chemical oscillation

and those involving more than one chemical oscillation. In this second type, of course, chemical oscillations inside each pattern exhibit different durations and amplitudes. In all cases, one can define a mean chemical period $\bar{P}_{ch} = (n/m)P_L$ which becomes $\bar{P}_{ch} = P_{ch} = nP_L$ when $m = 1$.

Fig. 6 is an illustration of the above-mentioned patterns. In fig. 6a and c, $m = 1$, and $n = 2$ and 1, respectively, whereas in fig. 6b and d, $m = 3$ and $n = 4$, and $m = 2$ and $n = 1$, respectively.

In the simplest case, $m = 1$ and $n = 1$ (fig. 6c), one chemical oscillation is achieved during exactly one photoperiod. It is the domain of fundamental forced oscillations. At photoperiods smaller than the free-running chemical period, two events simultaneously occur: the sudden jump of L from L_{min} to L_{max} and the reversal of the chemical potential evolution. In accordance with the observations related during perturbation experiments, this results in a natural decrease in not only the period but also the amplitude of the oscillations. Indeed, the application phase of the successive perturbations belongs to the advance-inducing zone of the oscillation. This behavior originates in the excitability property of these oscillations. At photoperiods longer than the free-running chemical period, the perturbations apply to a quite different phase region corresponding to a delay-inducing zone. As a result, the period and amplitude of the chemical oscillation are then increased to some extent. In all cases, before synchronization, a transient spell exists which extends over a variable number of oscillations. The application phase of the successive perturbations slips on the successive oscillations until it reaches a fixed phase value where it, henceforth, stabilizes. This is the so-called 'phase-locking' phenomenon.

In the case where $m = 1$ and $n = 2$ (fig. 6a), once every two $L_{min} \rightarrow L_{max}$ jumps apply at a phase belonging to the advance-inducing zone and the ohter applies in the refractory or delay-inducing zone. Analogous observations can be made for the next successive subharmonic forced oscillations when $n = 3, 4, 5, \ldots$.

When $m = 2$ and $n = 1$ (fig. 6d), P_L is long enough so that a whole chemical oscillation develops during the L_{min} irradiation time and an other shorter oscillation develops during the L_{max} irradiation time. In the same way, when P_L is increased, three of four chemical oscillations can develop during one photoperiod.

In the more complex case where $m = 3$ and $n = 4$ (fig. 6b), the observed repetitive patterns are composed of three chemical oscillations during

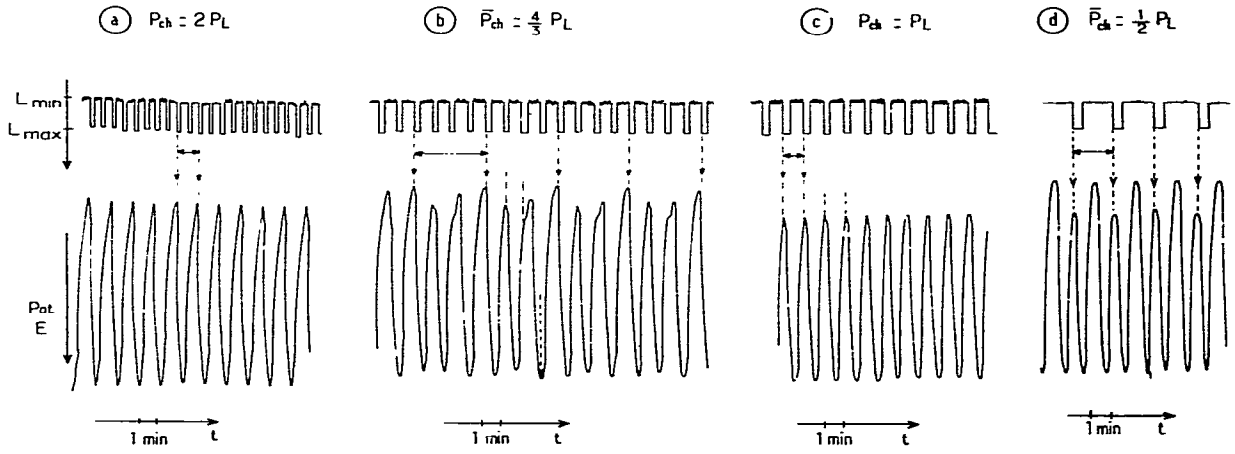

Fig. 6. Synchronization patterns for relaxation oscillations of composition β. Four different patterns obtained at constant $\bar{L} = 2$, $\rho = 1/4$, $\Delta L = 1$ and at four different P_L values: (a) $P_L = 36$ s, $n = 2$, $m = 1$; (b) $P_L = 63$ s, $n/m = 4/3$; (c) $P_L = 72$ s, $n = 1$, $m = 1$; (d) $P_L = 140$ s, $n/m = 1/2$.

four photoperiods. The oscillations have different amplitudes and durations. Indeed, the four successive perturbations apply at different phases of the three successive oscillations, thus inducing different phase shifts. This and other complex synchronization patterns, when established, can persist as long as the photoperiod remains unchanged, i.e., these complex patterns are stable. On the other hand, as seen in fig. 7, each n/m ratio exists over a certain range of P_L values. That is, every repetitive pattern of m oscillations has a certain domain of existence over P_L values. The broadest ones correspond to the simplest patterns, e.g., $n/m = 4/3$ or $3/2$ in fig. 7. The more complicated the patterns are, the narrower are the synchronization domains. Taking into account the limitations of our electronic clock, many of them are even reduced to a single P_L value. It is worth noticing in fig. 7 that the n/m ratio evolves stepwise as a function of P_L. Thus, many discrete fractional n/m values ($m > 1$) may be recognized between two successive n/m integer values ($m = 1$). As illustrated in fig. 7 and table 1, 13 fractional n/m values have been recognized between $n/1 = 2$ and $n/1 = 1$. The n/m value progressively evolves between 2 and 1. In the close vicinity of the domains where $m = 1$, very complicated oscillation patterns appear. Their stability was difficult to appreciate because they always extended over a great number of photoperiods. During these long runs, small fluctuations of our light source generally occurred. This can explain the lack of stability of some long patterns but does not completely exclude the possibility of intrinsic chaotic behavior [14]. A very well stabilized light source will enable us to distinguish between these two possibilities in a forthcoming study.

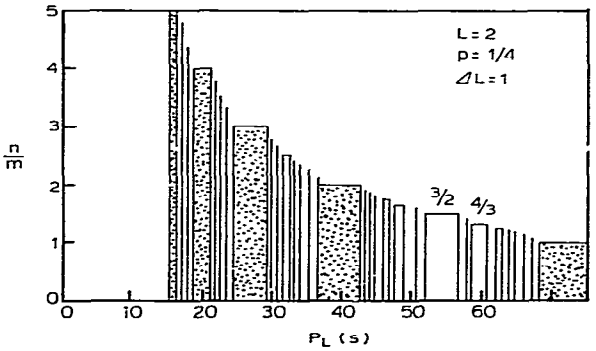

Fig. 7. n/m vs. P_L graph obtained under the same conditions as in fig. 6: $\Delta L = 2$, $\rho = 1/4$, $\Delta L = 1$. The n-integer domains have been shaded.

We finally illustrate in two different ways ($\bar{P}_{ch} = f(P_L)$ maps and $(\Delta L, P_L)$ constraint diagrams) five experiments, all performed at the same $\bar{L}$ and ρ values.

In the $\bar{P}_{ch}$ vs. P_L graphs (fig. 8), each domain of synchronization is a segment of a straight line issuing from the origin, with a slope of n/m. At high ΔL values ($\Delta L = 8$, 6, 4; fig. 8a–c), only segments with integer slope ($n/1$) can be seen. At low ΔL values ($\Delta L = 2$ and 1; fig. 8d and e), segments with fractional slope as well as segments with integer slope are observed. The $\bar{P}_{ch}$ vs. P_L graphs allow us to appreciate the modifications occurring in the chemical period under periodic light irradiation, i.e., the shift of the chemical period resulting from its synchronization by the photoperiod. At the lowest ΔL value ($\Delta L = 1$), the resulting $\bar{P}_{ch}$ always remains very close to 84 s, the free-runing P_{ch}^{L} value. Indeed, entrainment of the chemical period by these weak periodic perturbations is not very efficient and synchronization operates through a great number of complex patterns in such a way that $\bar{P}_{ch} = P_{ch}^{L}$.

As ΔL is increased, the number of complex synchronization patterns recognized between two successive simple patterns ($P_{ch} = n/1\ P_L$) decreases to the benefit of the latter domains whose extension, of course, increases. At sufficiently high ΔL, only simple $P_{ch} = nP_L$ patterns can be seen. It results from the fact that, going from one simple pattern, e.g., $n = 2$, to the next, say, $n = 1$, P_{ch} undergoes sudden jumps. For example, at this borderline, when $\Delta L = 8$, P_{ch} suddenly jumps from $P_{ch} = 2 \times 31.6\ \text{s} = 63.2\ \text{s}$ to $P_{ch} = 1 \times 32\ \text{s} = 32\ \text{s}$!

The segment with slope 1 is always much longer than any other. It allows us to appreciate the maximum entrainment capability of the light oscillator on the chemical oscillator. This can be easily done with the aid of table 2, for the five investigated ΔL values. Note that, as ΔL increases, the lower boundary of the fundamental synchroniza-

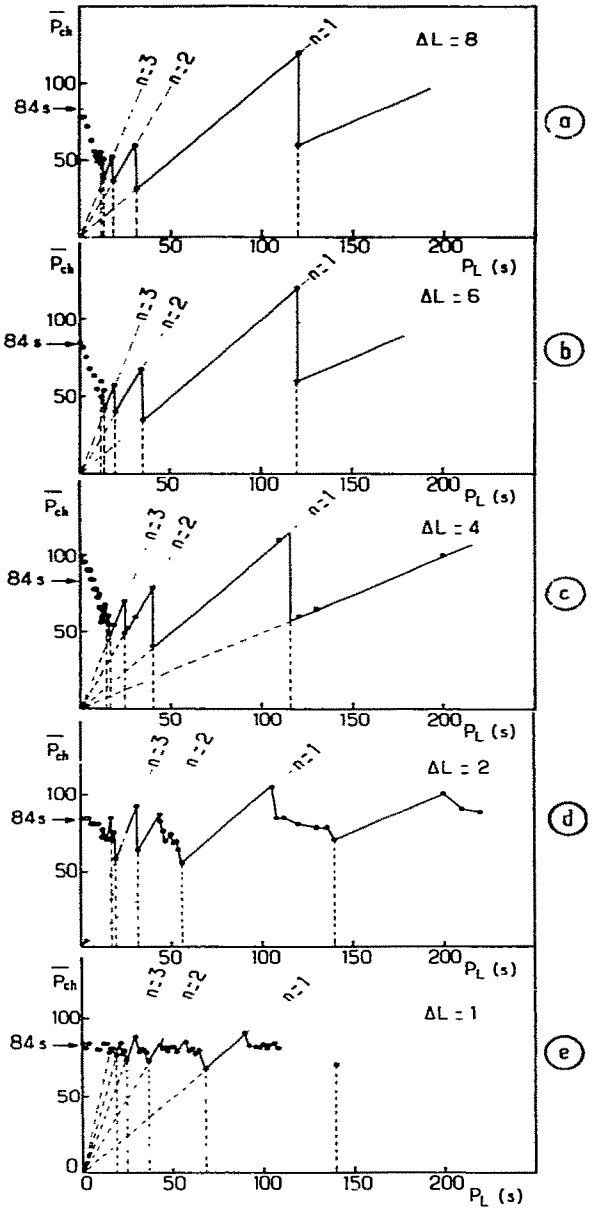

Fig. 8. $\bar{P}_{ch}$ vs. P_L graphs obtained at five different ΔL values. $\bar{L} = 2$, $\rho = 1/4$. The n values are indicated in the continuity of the corresponding n-sloped segments.

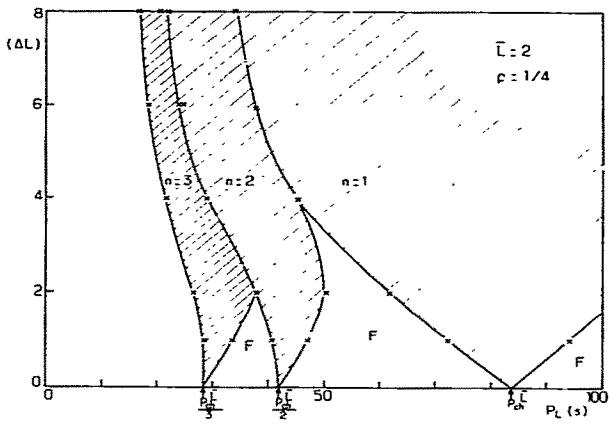

Fig. 9. $(\Delta L, P_L)$ Diagram obtained under the same conditions as in Fig. 8: $\bar{L} = 2$, $\rho = 1/4$. The shaded zones are the domains of existence of the simplest patterns ($n/1 = 3, 2, 1$). The F zones gather the domains of existence of complex n/m patterns between $n/1 = 3$ and $n/1 = 2$ and between $n/1 = 2$ and $n/1 = 1$.

tion domain shifts towards shorter photoperiods.

In the $(\Delta L, P_L)$ constraint diagram (fig. 9), the various synchronization domains are delimited as a function of ΔL and P_L. On the one hand, these are the $n/1$ integer domains (for the sake of clarity, only the $n = 1, 2, 3$ domains are shown). On the other, the 'F' domains correspond to the various fractional n/m values. This diagram offers a general but simplified view of the situation: (i) at high ΔL, only synchronization patterns with $m = 1$ are observed; (ii) the $n/1$ integer domains shift towards longer photoperiods as ΔL is decrease; (iii) as ΔL is decreased, the various $n/1$ domains focus towards the corresponding P_{ch}^{L}/n values. It is thought that every synchronization domain of gen-

Table 1

n/m	2/1	17/9	15/8	9/5	7/4	5/3	8/5	3/2	7/5	4/3	5/4	6/5	9/8	13/12	1/1
dec	2	1.89	1.87	1.80	1.75	1.66	1.60	1.50	1.40	1.33	1.25	1.20	1.12	1.08	1

Table 2

Conditions: $\bar{L} = 2$, $\rho = 1/4$.

ΔL	Variation domain of P_L (s)
8	32–120
6	35–120
4	40–115
2	55–110
1	68– 90

eral form $m\bar{P}_{ch} = nP_L$ (with $m \geqslant 1$) will focus towards $P_L = (m/n)P_{ch}^{\bar{L}}$ as ΔL decreases to zero. This makes sense, since at $\Delta L = 0$, i.e., under continuous light irradiation, the system must return to its free-running period.

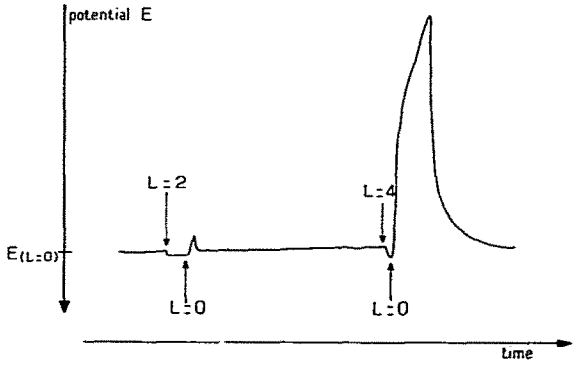

Fig. 10. Effects of a light flux jump on the stationary state: a jump $\Delta L = 2$ (from $L = 2$ to $L = 0$) is inefficient, after a jump $\Delta L = 4$ (from $L = 4$ to $L = 0$); an excitability peak appears.

3. Effect of periodic light irradiation of an excitable stable steady state

The stationary state studied is located in the close vicinity of the oscillating state of composition β described above. This state is stationary in the dark and under continuous light irradiation.

A single light pulse is, nevertheless, able to induce a large deviation of the potential before it returns to its initial level. This large potential change corresponds to an 'excitability peak'. It happens just as the light flux is shut off, provided the L jump ($L_{max} \rightarrow L = 0$) is large enough (fig. 10). Thresholds are characteristic of excitable states. Here, the threshold value is $\Delta L = 4$. For any $\Delta L < 4$, the system returns immediately to its steady potential whereas for any $\Delta L > 4$ a large excitability peak appears with a characteristic amplitude and duration independent of ΔL. The excitability peak is similar to a relaxation oscillation seen in the neighboring oscillation domain.

When studying the effects of periodic light pulses on this stationary state, the light parameters values were set to $\bar{L} = 2$, $\rho = 1/10$, $\Delta L = 20$ ($L_{min} = 0$, $L_{max} = 20$), and P_L variable. Note that the ΔL value chosen here is much larger than the threshold value determined above. Fig. 11 shows some of the results obtained for increasing P_L values. For large P_L ($P_L \geqslant 180$ s) one observes an excitability peak at every P_L, i.e., there is direct synchronization of the excitability peak on the photoperiod. At P_L values immediately below (160 s $\geqslant P_L \geqslant$ 50 s), a peak of excitability is observed every two photoperiods, i.e., there is again synchronization but the second light pulse occurs during the refractory phase of the excitability peak. Similar observations can be made at $P_L = 40$ s, but there every excitability peak involves five or six photoperiods. At $P_L = 30$ s, excitability peaks emerge only from time to time whereas, for $P_L = 20$

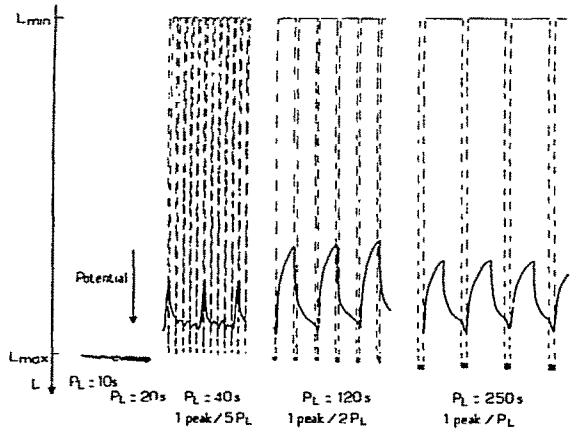

Fig. 11. Effects of periodic light pulses (period P_L) on the same stationary state as in fig. 10, with $\Delta L = 20$ and $\rho = 1/10$. (— — —) Light flux, L; (————) potential, E.

s. no response at all is osberved, the system only seeming to 'see' a mean light flux.

It thus appears that, in accordance with the threshold properties of excitability, a minimum duration of the light pulses is also necessary to induce an excitability peak (note that, because ρ is kept constant, $t_{L_{max}}$ decreases with P_L). Note also that a photoperiod of 50 s is able to entrain this chemical system on a 100 s period which is much lower than the direct one on one entrainment whose lower boundary is near 160 s. This implies that a low P_L values, there is the possibility of an accumulation effect of the periodic perturbations, in other words, the chemical system does not completely recover between the successive apparently inefficient light pulses.

It must also be emphasized that, although in the set of experiments reported above only simple synchronization patterns were presented, more complex n/m patterns with $m > 1$ (have also been recognized at lower ΔL values, just as in the previously described relaxation oscillation state.

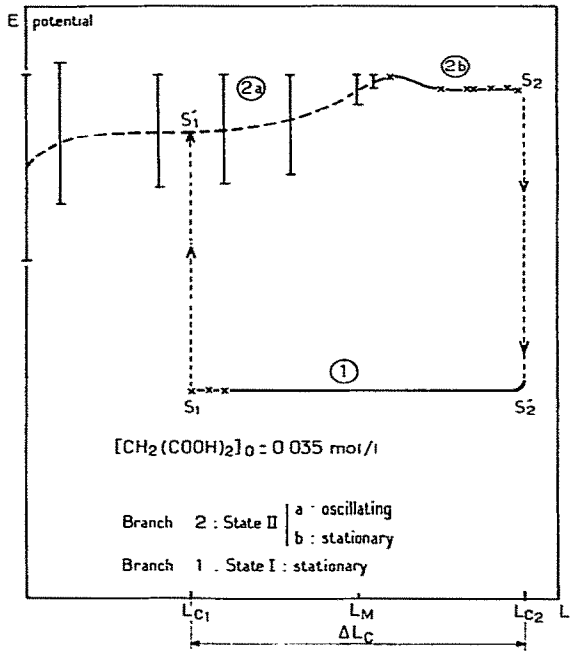

Fig. 12. Potential bistability as a function of continuous light irradiation. Vertical segments give the amplitude of oscillations on branch 2.

4. Effect of periodic irradiation on a bistable system

Several bistable regions are known [8] in the B.R. reaction. In the following experiments, we shall focus our attention on a composition exhibiting hysteresis phenomena as a function of the continuous light flux value L. The following constraint values were retained: $[CH_2(COOH)_2]_0 = 0.035$ mol/l, $[KIO_3]_0 = 0.047$ mol/l, $[H_2O_2]_0 = 1$ mol/l, $[HClO_4]_0 = 0.056$ mol/l, $[MnSO_4]_0 = 0.004$ mol/l; $T = 24.5$°C and $\theta_r = 3$ min. These experimental conditions are close to those chosen earlier by De Kepper and Horsthemke [15] to study noise-induced transitions.

In fig. 12, the redox potential response is plotted as a function of a continuous light flux L. Bistability is observed between a low-potential steady state (state I) and a high-potential oscillating state (state II). In the dark ($L = 0$), the system is in state II, the vertical segments represent the amplitude of the oscillations. As L is increased, this amplitude decreases and oscillations are completely abolished beyond $L = 10.5$. Thereafter, a high-potential steady state remains until the light flux reaches the critical value $L = 15$ where the system undergoes a transition towards the low-potential steady state I. If L_{C_2} is now decreased, the system remains in this low-potential state until the light flux reaches another critical value $L_{C_1} = 5$ where the system unergoes the reverse transition towards state II. Thus, for any value $5 \leqslant L \leqslant 15$, the system may be in either of the two states I or II, the actual observed state depending only on its preceding history. For a better understanding of the following experiments, note that this bistable system has two critical transition values $L_{C_1} = 5$ and $L_{C_2} = 15$, a width $\Delta L_C = L_{C_2} - L_{C_1} = 10$, centered on $L_M = 10$, and that the characteristic transition times τ between the two states are $\tau_{II \to I} = 2.5$ min and $\tau_{I \to II} = 7$ min,

Extensive studies of this bistable system were made under the following periodic light irradiation conditions: $\bar{L} = L_m = 10$ and $\rho = 1/2$. The results

in the $(\Delta L, P_L)$ constraint plane are shown in fig. 13. We may distinguish four regions.

Region b, where both states I and II are possible, is the natural extension of the bistable properties of the system at continuous light irradiation. This region essentially corresponds to the low ΔL values, i.e., $\Delta L < \Delta L_c$, which do not allow any spontaneous transition from state I to state II or vice versa. The system will be in state I when shifted from region a and in state II if previously in region d. At low P_L, the bistable region extends over values of $\Delta L > \Delta L_C$, probably because in this part, the system spends too short a time just beyond the light flux transition boundaries.

In region a, only state I exists. In this region, $\Delta L \gg \Delta L_c$, the system is pulled alternately beyond each transition boundary. But, because P_L is short and $\tau_{II \to I}$ smaller than $\tau_{I \to II}$, the stability of state I is favored.

In region c, induced oscillations are observed. Indeed, region c corresponds to large-magnitude perturbations and long photoperiods, thus allowing the system to drift along one branch of the bistable system and undergo a transition during the time the light flux is at its maximum and then to drift and jump back when L is at its minimum.

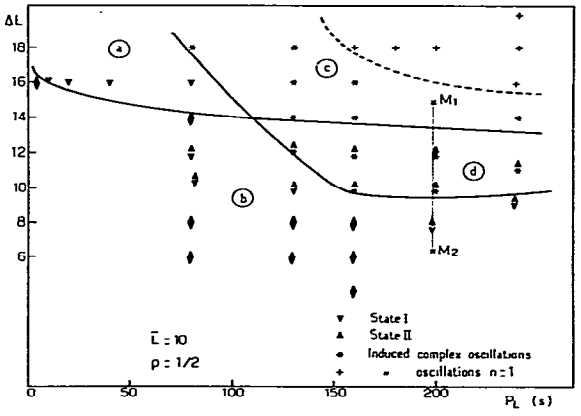

Fig. 13. Phase diagram $(\Delta L, P_L)$ obtained when the bistable system is under periodic light irradiation ($\bar{L} = 10$, $\rho = 1/2$). Four regions: (a) only state I is stable, (b) state I and state II are stable, (c) induced relaxation oscillations (complex patterns (*) or simple pattern (+)), (d) state II and induced relaxation oscillations.

Thus, periodic perturbations will induce periodic runs around the hysteresis cycle. They can be thought of as relaxation oscillations and they are naturally synchronized with the photoperiods. However, here again, we can observe different types of synchronization patterns, depending on the ΔL and P_L values. In the upper right-hand corner, direct synchronization is observed ($P_{ch} = 1/1\ P_L$). As shown in fig. 14a, these induced oscillations are the combination of large induced oscillations and small oscillations belonging to state II. Just below, more complex synchronization patterns are observed, as shown in fig. 14b. Notice the strong similarity between this behavior and that previously observed for both relaxation oscillations and the excitable state.

Region d corresponds to bistability between steady state II and induced oscillations.

The total resulting domain of induced oscillations includes regions c and d. It has an asymptotical limit for long P_L, at $\Delta L = \Delta L_c = 10$. When P_L is shorter than any of the characteristic transition times, the system still exhibits induced oscillations for $\Delta L \gg \Delta L_c$. This can be understood by the fact that the further the system is pulled from its critical bistable values, the faster the transitions to each state occur. This phase diagram bears some similarity to the cross-shaped diagrams described

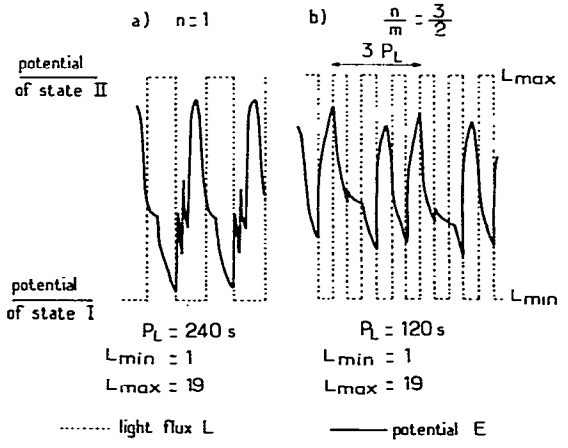

Fig. 14. Oscillation diagrams induced in regions c and d on fig. 13. (a) $n = 1$, simple pattern but composite oscillations; (b) $n/m = 3/2$, two oscillations during three photoperiods.

by Boissonade and De Kepper [16] in systems compounded of a bistable and of a feedback subsystem, but here it is the external periodic change in light flux that plays a role similar to the feedback in their cross-shaped diagram.

5. Discussion

Let us now compare, at the phenomenological level, our experimental results with those obtained for biological oscillators subjected to similar experimentation.

Perturbation (or 'phase resetting') experiments, using single perturbations, are commonly carried out in order to test the sensitivity of biological clocks to their environment. Let us mention, among others, typical examples of the rhythmic eclosion of the flesh fly *Drosophila Pseudoobscura* [17,18], the alternating opening and closing of the flower of *Kalanchoe Blossfeldiana* [18,19], the cellular oscillator of the periodically agregating slime mould *Dictyostelium Discoideum* [20], and the rhythmic firing of neuronal [21] and cardiac [12] pacemakers. The results are usually gathered in phase-response curve representations resembling those in fig. 4, with refractory zones, delay- and advance-inducing zones, sometimes separated by discontinuities.

In fact, as pointed out by Winfree [18], there are, in the literature, notable differences in the definition of advance and delay, which caused some confusion in the significance of discontinuities eventually appearing in the phase-response curve representations. Do these discontinuities correspond to real physiological jerks linked to the oscillator mechanism? Or are they only artefacts of the representation? Both cases are encountered.

In our experiments in fig. 4, the discontinuity between the refractory (or the delay-inducing) zone and the advance-inducing zone indubitably originates in the marked excitability character of the oscillation of composition β. This discontinuity increases with the size of the perturbation, to reach a maximum value equal to a whole cycle for $S = 32$ s.

Artefactual discontinuities, in some biological studies [17–19], are introduced by the way delays and advances are evaluated: in such cases, the phase shift is measured as the difference, in cycle units, between the time of a reference event in the perturbed oscillator and the time of the nearest reference event in the undisturbed control oscillator. This convention, obviously, infers that no advance (or delay) can be greater than half a cycle: indeed, if an advance (delay) is greater than half a cycle, it would appear as a delay (advance) of the previous (following) cycle. This arbitrary distinction between delay and advance can introduce a discontinuity of a whole cycle amplitude between delay- and advance-inducing zones, without physical significance. As a matter of fact, such a definition would change into delays part of what we have determined as advances in fig. 4.

In order to avoid such an inconsistency in the representation of the phase-resetting experiment, Winfree [11] tends to adopt another graphic form: the 'new phase vs. old phase' maps. But, in this type of representation, there is a loss of information: first, it evades the problem of advance and delay, which are not just relative notions, as we have shown; second, it does not allow direct prediction of the entrainment capability of the oscillator.

From both considerations, it results that the phase-response curve representation, as used in fig. 4, is more desirable. For a correct reading of the phase shift as delay or advance, one must number the cycles (or reference events) which have occurred since the time of perturbation. The phase shift must then be measured between cycles of the same rank (see fig. 3) in the perturbed and unperturbed oscillators.

Periodic forcing of biological oscillators is currently used in biological studies whether it is for an economic goal (increase in the egg yield of hens) or for medical purposes (cardiac stimulators). The major results are similar to those we have observed in the chemical oscillator but the different phenomena observed in our set of experiments are more or less scattered over a large number of different systems. Some of the most thorough entrainment studies were made in the case of neuronal [22] and cardiac [12] pacemakers submitted to periodic stimuli. They show fundamental entrainment as well as harmonic and subharmonic en-

trainment in the same way the chemical composition β does: at large perturbation size, in the case of ref. 22, or at small perturbation size, in the case of ref. 12. Moreover, in the latter case, chaotic behavior has also been evidenced at particular values of the forcing frequency. Let us also mention the case of the $n/1$ synchronization patterns observed in the glycolytic oscillator subjected to periodic variations of the substrate rate injection [23], and the large domain of entrainment of the Kalanchoe petal rhythm on periodic red-light pulses [19]. It is worth noticing that the behavior of all these biological oscillators, easily forced over large domains of frequencies, is more consistent with the observations made on composition β than those on ocmposition α, which suggests that most biological oscillators have highly nonlinear dynamics.

6. Conclusion

It appears that either relaxation oscillations, steady excitable state or bistability, can lead to the same types of synchronization patterns when submitted to periodic perturbations. The main common character of these three phenomena is the existence of threshold values for the perturbation. In the relaxation oscillations, this is made evident through the discontinuity in the phase-response curve, whereas, the existence of a threshold perturbation value in the recovery dynamics of a steady state defines an excitable state. In the bistable system, the critical values of the hysteresis loop correspond to two threshold values. Thus, there is no need for an intrinsic periodic clock for a system to exhibit adaptation to an external periodic force. The remark is important when studying entrainment phenomena in nature. We have shown, in fact, that excitable steady states and bistable systems could also act as time dividers when submitted to periodic perturbations. The only sensible way to distinguish between these three possibilities is then of course, when possible, to study the system freed from its periodic forcing. Note also that most known biological self-oscillating systems exhibit responses to single perturbations or entrainment capability consistent with that of nonlinear excitable oscillators.

References

1 T. Van den Riessche, Colloq. Int. CNRS 240 (1975) 33.
1 a L.N. Edmunds, Jr, R.I. Apter, P.J. Rosental, W.K. Shen and J.R. Wooward, Photochem. Photobiol. 30 (1979) 595.
1 b L.N. Edmunds, Jr, Col'oq. Int. CNRS 240 (1975) 53.
2 T. Van den Driessche, Biosystems 6 (1975) 188.
3 J. Brulfert, D. Guerrier and O. Queiroz, Planta 125 (1975) 33.
4 T.S. Briggs and W.C. Rauscher, J. Chem. Educ. 50 (1973) 496.
5 a P. De Kepper and I.R. Epstein, J. Am. Chem. Soc. 104 (1982) 49.
5 b S. Furrow and R.M. Noyes, J. Am. Chem. Soc. 104 (1982) 45.
6 P. De Kepper, A. Pacault and A. Rossi, C.R. Acad. Sci. Paris 282C (1976) 199.
7 P. De Kepper, C.R. Acad. Sci. Paris 283C (1976) 25.
8 P. De Kepper, Ph.D. Thesis, Bordeaux, France (1978).
9 E. Dulos, Ph.D. Thesis, Bordeaux, France (1981).
10 J.E. Marsden and M. McCraken, The Hopf bifurcation and its application (Springer-Verlag, New York, 1976).
11 A.T. Winfree, in: Biological and biochemical oscillators, eds. B. Chance, K.E. Pye, A.K. Ghosh and B. Hess Academic Press, New York, 1973) p. 461.
12 M.R. Guevara, L. Glass and A. Shrier, Science 214 (1981) 1350.
13 G.P. Moore, D.H. Perkel and J.P. Segundo, in: Proceedings of the San Diego Symposium for Biomedical Engineering, ed. (A. Paull (1963) p. 184.
14 Ann. N.Y. Acad. Sci. 357 (1980).
15 P. De Kepper, W. Horsthemke, C.R. Acad. Sci. Paris 287C (1978) 251.
16 J. Boissonade, P. De Kepper, J. Chem. Phys. 84 (1980) 501.
17 C.S. Pittendrigh, D.H. Minis, Am. Nat. 98 (1964) 261.
18 A.T. Winfree, The geometry of biological time (Biomathematics, vol. 8 (Springer-Verlag, Berlin, 1980) p. 383.
19 W. Engelmann, H.G. Karlsson and A. Johnsson, Int. J. Chronobiol. 1 (1973) 147.
20 A. Johnsson, H.G. Karlsson and W. Engelmann, Physiol. Plant. 28 (1973) 132.
21 G. Gerish, D. Malchow, W. Ross and U. Wick, J. Exp. Biol. 81 (1979) 33.
22 H.M. Pinsker, J. Neurophysiol. 40 (1977) 527.
23 D.H. Perkel, J.H. Schulmann, T.H. Bullock, G.P. Moore and T.P. Segundo, Science 145 (1964) 61.
24 A. Boiteux, A. Goldbetter and B. Hess, Proc. Natl. Acad. Sci. U.S.A. 72 (1975) 3829.